

Direct Waves in Black-Hole Binary Mergers: Insights from the Backwards One Body Model

Anuj Kankani^{1,2,*} and Sean T. McWilliams^{1,2}

¹*Department of Physics and Astronomy, West Virginia University, Morgantown, WV 26506, USA*

²*Center for Gravitational Waves and Cosmology, West Virginia University,
Chestnut Ridge Research Building, Morgantown, WV 26505, USA*

(Dated: March 17, 2026)

The merger-ringdown radiation from a black hole binary merger is accurately modeled by a sum of linear quasinormal modes (QNMs). Recently, a non-QNM “direct wave” component of the radiation, associated with prompt emission from a plunging perturber, has been identified. Motivated by the behavior of null geodesics perturbed from the remnant light ring, the Backwards One Body (BOB) approach has been shown to model the full merger-ringdown radiation to high accuracy, while using only a minimal number of parameters. In this work, using the Pöschl–Teller potential, we first show how the BOB amplitude evolution can be recovered from the QNM pole contributions. We then apply rational filters to isolate the non-QNM content in BOB and numerical relativity waveforms. We show that BOB naturally captures the direct wave component of the merger radiation, explaining its accuracy near the waveform peak. Finally, we use BOB to show that the direct wave frequency is largely uncorrelated with the horizon frequency, even for high spin remnants, and instead tracks the News frequency at the time of the peak News amplitude.

Introduction.— The merger and ringdown radiation emitted from a black hole binary merger provides a direct probe for testing General Relativity (GR) in the strong field regime. The ringdown phase is described by black hole perturbation theory [1–6] and can be accurately modeled as a sum of linear quasinormal modes [7–11]. Additionally, there has been evidence for the presence of non-linear QNMs in numerical relativity (NR) waveforms [12–17], as well as late time tails [18–20]. Recently, a distinct non-QNM contribution to the merger radiation, the “direct wave” [21], was identified through the application of rational filters [22–25], which allow for the removal of QNM content without requiring any fitting.

Another approach to modeling the merger-ringdown radiation is the Backwards One Body (BOB) model [26–29]. Based on the behavior of a packet of null geodesics perturbed from the light ring of the remnant black hole [6, 26], BOB produces a hyperbolic-secant amplitude evolution and has been shown to model NR merger-ringdown News waveforms with high accuracy for quasi-circular and non-precessing cases across the SXS catalog while requiring only a minimal number of parameters [27]. Although BOB is distinct from a sum of QNMs, it shares several important features with QNM-based descriptions. In particular, at late times its amplitude evolution approaches that of the fundamental QNM, leading to analytic relations between the peak News amplitude and the fundamental mode excitation [27, 30]. Importantly, BOB performs significantly better than a QNM sum prior to the peak while using far fewer free parameters [27].

Despite its empirical success, the physical origin of BOB’s remarkable accuracy near the waveform peak remains unclear. In this Letter we clarify the origin of this behavior. First, using the Pöschl–Teller potential [31], we show that the QNM pole contributions produce the

hyperbolic secant amplitude profile predicted by BOB. Then, applying rational filters to both BOB and NR waveforms, we demonstrate that BOB naturally captures the non-QNM direct-wave component of the merger radiation. Taking advantage of BOB’s analytical form, we explore properties of the direct wave frequency across the parameter space and show that even for high spin systems, it is largely uncorrelated with the horizon frequency of the remnant black hole. Rather, we find a strong correlation with the News frequency at the time of the peak News amplitude.

A QNM approach to BOB.— While BOB shares many similarities to a sum of linear quasinormal modes, it only directly matches a QNM description at late times, when only the fundamental mode remains [27, 30]. BOB matches the accuracy of 4–5 QNMs at the peak of the waveform, while requiring significantly fewer free parameters, and retains better behavior before the peak [27]. The original BOB derivation was based on the divergence of null rays from the remnant black hole [6, 26]. To gain further intuition into the connection between BOB and QNMs, we follow a more standard QNM derivation procedure based on the Sasaki–Nakamura (SN) formalism [32, 33]. We only provide a brief overview of the standard QNM portion of the derivation, referring readers to [33] for more details. Perturbations induced by a spin- s field are described by a function $X^{(s)}(t, r)$ whose Laplace transform satisfies

$$\frac{d^2 \hat{X}^{(s)}(\omega, r)}{dr_*^2} + V_{\text{eff}}(r) \hat{X}^{(s)}(\omega, r) = I(\omega, r), \quad (1)$$

where r_* is the tortoise coordinate, $V_{\text{eff}}(r)$ is an effective potential, and $I(\omega, r)$ represents the initial data. Assuming the observer is located far from the black hole, we obtain the standard description of the ringdown as a

sum of quasinormal modes [5].

$$X^{(s)}(t, r) = -\operatorname{Re} \left[\sum_n C_n e^{-i\omega_n(t-r_*)} \right], \quad (2)$$

where C_n are quasinormal excitation coefficients, represented as the product of the quasinormal excitation factor B_n and an integral over the source I_n , $C_n = B_n I_n$. Additional details are provided in the supplemental materials. Because the exact form of the initial data sourcing QNMs for astrophysically realistic mergers is unknown, in practice the QNM amplitudes are obtained by fitting to a known waveform. The BOB approach to merger-ringdown modeling suggests that the initial data is uniform across each ω_n , with the effect of the initial data being captured by the amplitude A_p . Furthermore, several studies analyzing NR waveforms have found evidence that the source term for prograde QNMs is largely independent of the overtone index n [7, 8, 34, 35]. This assumption greatly simplifies the analytical study of the merger-ringdown radiation and allows us to gain insight into why BOB successfully models the merger-ringdown radiation. Under the assumption that prograde QNMs have, to a good approximation, a common source term, we can rewrite Eq. (2) as

$$X^{(s)}(t, r) \propto \operatorname{Re} \left[\sum_n B_n e^{-i\omega_n(t-r_*)} \right]. \quad (3)$$

We employ the Pöschl–Teller (PT) potential [6, 31, 36], a common substitution for the true Regge–Wheeler potential due to its simpler analytic structure.

$$V_{\text{PT}} = \frac{V_0}{\cosh^2 \alpha(x-x_0)}, \quad (4)$$

where $\tau = 2/\alpha$ is the inverse of the imaginary part of the fundamental QNM. Converting the master variable $dX^{(s)}/dt$ to the News, we find for the PT potential

$$|\mathcal{N}_+(t) - i\mathcal{N}_\times(t)| \propto \operatorname{sech} \left(\frac{t-t_p}{\tau} \right) |F(t)|, \quad (8)$$

where x_0 is the location of the maximum, V_0 is the height of the potential and α is related to the second derivative of V_{PT} . Because we are primarily concerned with the behavior of the potential around the peak, where the PT potential can be tuned to mimic the true effective potential, it is an accurate approximation for our calculation. Based on the reflection and transmission coefficients of the PT potential, calculated in [6], the quasinormal excitation factors B_n were calculated explicitly in [33]¹ as

$$B_n^{\text{PT}} = \frac{i\alpha(-1)^{n+1}\Gamma(n-\beta)\Gamma(1+2\beta-n)}{2\omega_n n! \Gamma(1+\beta)\Gamma(-\beta)\Gamma(\beta-n)}, \quad (5)$$

where $\beta = -1/2 + \sqrt{1/4 - V_0/\alpha^2} \equiv -1/2 + i\delta$. The QNM can be identified from the poles in the reflection and transmission coefficients as $\omega_n = i\alpha\sqrt{1/4 - V_0/\alpha^2} - i\alpha(n+1/2)$ [6, 33]. Based on comparisons to NR waveforms, [27] argued that the BOB amplitude evolution best represents the gravitational wave News, \mathcal{N} , while $X^{(s)}$ is more directly related to the gravitational wave strain, h . Differentiating the above result and substituting B_n^{PT} results in

$$\frac{dX^{(s)}(t, r)}{dt} \propto \operatorname{Re} \left[\frac{\alpha}{2\Gamma(1+\beta)\Gamma(-\beta)} \left[\sum_n \frac{(-1)^n \Gamma(n-\beta)\Gamma(1+2\beta-n)}{n! \Gamma(\beta-n)} e^{-i\omega_n(t-r_*)} \right] \right]. \quad (6)$$

Employing the identities $\Gamma(z-n) = (-1)^n \Gamma(z)/(1-z)_n$ and $(x)_n = \Gamma(x+n)/\Gamma(x)$ where $(x)_n$ is the Pochhammer symbol, allows us to rewrite the series as a hypergeometric function $F(a, b; c; z)$ [37]. Using the identity $F(a, b; c; z) = (1-z)^{c-a-b} F(c-a, c-b; c; z)$, we obtain

$$\begin{aligned} \frac{dX^{(s)}(t, r)}{dt} &\propto \operatorname{Re} \left[\frac{\alpha\Gamma(1+2\beta)}{2\Gamma(\beta)\Gamma(1+\beta)} e^{+\alpha\beta(t-r_*)} (1+e^{-\alpha(t-r_*)})^{-1} F \left(-\beta, -1-\beta; -2\beta; -e^{-\alpha(t-r_*)} \right) \right] \\ &\propto \operatorname{Re} \left[\operatorname{sech} \left(\frac{t-r_*}{\tau} \right) e^{i\alpha\delta(t-r_*)} F \left(\frac{1}{2} - i\delta, \frac{-1}{2} - i\delta; 1 - 2i\delta; -e^{-\alpha(t-r_*)} \right) \right] \end{aligned} \quad (7)$$

under the assumption that for non-spinning systems in the eikonal limit $c_0 \propto l^2$ [32, 33, 38]. Here we have suppressed the (l, m) dependence, $F(t)$ is the specific hypergeometric function appearing in Eq. (7), and we have used $t-r_* \equiv t-t_p$. Noting that the hypergeometric function appearing in Eq. (7) is a sum of exponentially damped terms, we treat $|F(a, b; c; -e^{-\alpha(t-r_*)})|$ as a constant. We provide greater detail on the conversion from $X^{(s)}$ to \mathcal{N} and our approximation of the hypergeometric function in the supplemental materials. This results in an amplitude profile exactly matching that from the original

¹ There is a sign error in appendix A3 of [33] due to the opposite sign convention for ω in [6]. The B_n^{PT} expression remains unchanged, but the correct pole condition is $-\beta - i\omega/\alpha = -n$.

derivation based on the perturbations of null geodesics from the light ring.

$$|\mathcal{N}(t)| \propto \operatorname{sech}\left(\frac{t-t_p}{\tau}\right), \quad (9)$$

Importantly, reproducing the hyperbolic secant profile involves $dX^{(s)}/dt$, rather than $X^{(s)}$, complementing the empirical evidence provided in [27] that BOB fundamentally models the News, rather than Ψ_4 as was originally suggested in [26]². While we have limited ourselves to the PT potential, the success of BOB across the SXS catalog [27], where the Kerr ($s = -2, l = 2, m = 2, n = 0$) QNM is used, suggests that physical insight gained in the simpler PT potential translates well to the full Kerr potential.

Studying BOB with Rational Filters.— Rational filters [22, 24, 25], which work in the frequency domain, help remove QNM content from merger-ringdown waveforms without requiring any fitting. Rational filters were employed in [21] to identify the presence of a distinct non-QNM component of the merger radiation, the “direct wave”, associated with the direct emission from the plunging perturber [21].

As shown in [27], BOB’s amplitude evolution incorporates information from an infinite number of overtones in the eikonal limit. BOB’s accuracy near and before the peak of the waveform strongly suggests it is modeling more than the linear QNM content of the merger-ringdown radiation. In this section, we explore this idea through the application of rational filters on BOB waveforms.

We focus our analysis on three quasicircular and non-precessing NR simulations. The first, SXS:BBH:0305 [39–42], has parameters similar to GW150914 [43], and was analyzed with rational filters in [21, 24]. The second, SXS:BBH:4123 [40–42, 44], consists of a $q = 4$ mass ratio system with a highly spinning remnant, $\chi_f = 0.915$. The last simulation, SXS:BBH:2477 [40–42, 45, 46], consists of a $q = 15$ mass ratio system with a low spin remnant, $\chi_f = 0.189$. Because BOB most accurately models the gravitational wave News [27], we apply rational filters to the News rather than the strain. The News contains the same QNM frequencies as the strain; therefore, the same rational filters apply. For the NR simulations, following [21], we remove 7 prograde, 2 retrograde and the (3,2) mode. For BOB, we employ two approaches. The first is to remove the exact same QNMs from BOB that we do from the NR waveform. In the second approach, we account for how BOB incorporates overtone information into its amplitude evolution. The BOB amplitude evolu-

tion can be rewritten as

$$\begin{aligned} A_p \operatorname{sech}\left(\frac{t-t_p}{\tau}\right) &= 2A_p \sum_{n=0}^{\infty} (-1)^n e^{-(2n+1)\frac{t-t_p}{\tau}} \\ &= 2A_p \left(e^{-\frac{t-t_p}{\tau}} - e^{-3\frac{t-t_p}{\tau}} + e^{-5\frac{t-t_p}{\tau}} + \dots \right). \end{aligned} \quad (10)$$

From this, we can see that BOB incorporates the damping times of overtones through the eikonal limit where $\tau_n = \tau_{n=0}/(2n+1)$. Therefore, in our second approach to filtering BOB, we only remove seven prograde QNMs. The imaginary part of the overtones is incorporated through the eikonal limit. The fundamental mode, and the real part of the QNMs, use the values determined from the `qnm` package [47].

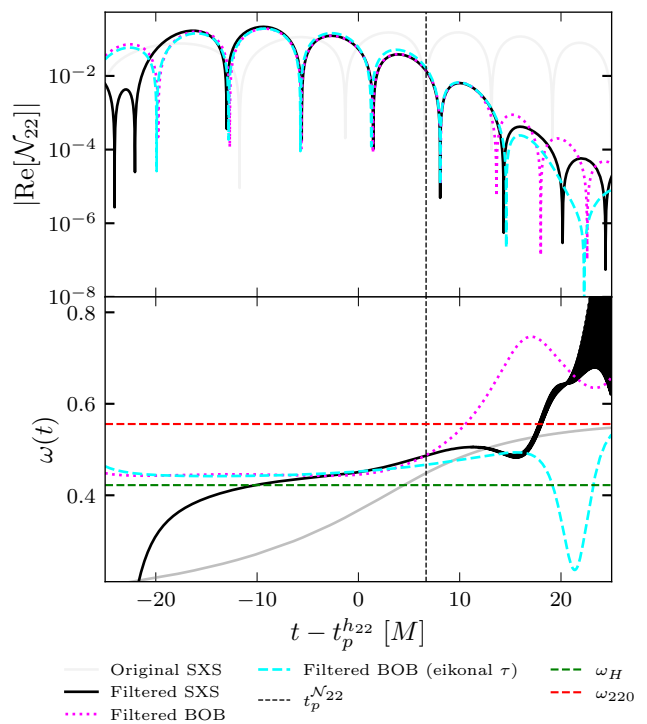


FIG. 1: Top: Filtered NR News (SXS:BBH:0305 [39–42]) waveform (solid black) compared to a filtered BOB waveform with the exact same QNMs removed (dotted red) and an “eikonal filtered” BOB waveform (dashed cyan). In light grey we plot the original NR waveform. Bottom: Instantaneous waveform frequency for the filtered waveforms. We also plot the `qnm` frequency (dashed green) and $\omega_H = 2\Omega_H$, where Ω_H is the horizon frequency (dashed red).

In Figs. (1) - (3), we compare filtered BOB waveforms and NR waveforms. While we filter the gravitational wave News, our axis is with respect to the original strain peak for easier comparison to other work. The three SXS waveforms compared here were chosen to span

² Although, as has been shown in [26] and [27], the BOB amplitude and frequency profile can still model Ψ_4 accurately.

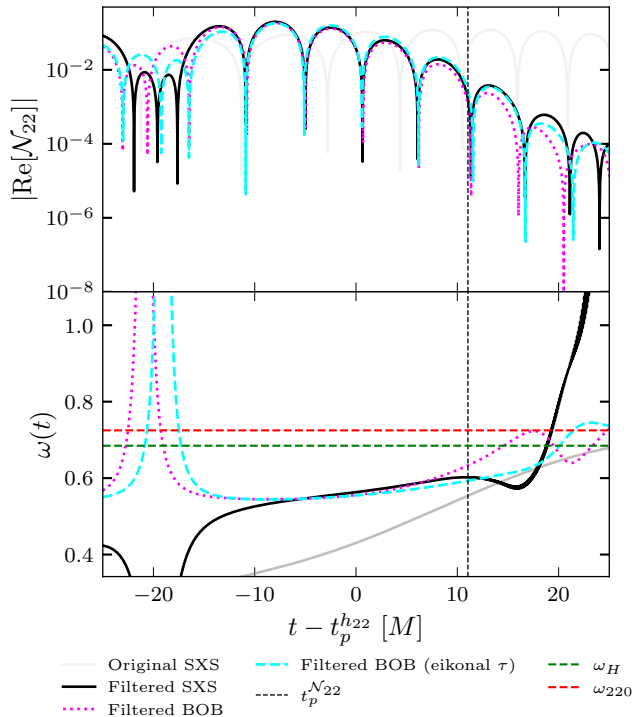


FIG. 2: Top: Filtered NR News (SXS:BBH:4123 [40–42, 44]) waveform (solid black) compared to a filtered BOB waveform with the exact same QNMs removed (dotted red) and an “eikonal filtered” BOB waveform (dashed cyan). In light grey we plot the original NR waveform. Bottom: Instantaneous waveform frequency for the filtered waveforms. We also plot the qnm frequency (dashed green) and $w_H = 2\Omega_H$, where Ω_H is the horizon frequency (dashed red).

a wide range of initial mass ratios and remnant spins. In all three cases, we find excellent agreement between the filtered NR waveform and the filtered BOB waveforms. We find agreement over a period of $10 - 30M$, depending on the system parameters and the filtering strategy. Surprisingly, we find that BOB and NR filtered waveforms can agree as far back as $15M$ before the strain peak and up to $20M$ after the strain peak. Furthermore, BOB successfully models this non-QNM component across a wide variety of initial mass ratios and remnant spins. In Figs. (1) - (3), we also plot the waveform frequency for the filtered waveforms. We can observe when we incorporate the eikonal limit in the damping time of overtones, the BOB filtered frequency shows very little evolution during the period of agreement. Applying the exact same filter to BOB that we apply to the NR waveforms, we find once again that there is very little evolution before the News peak, but after the News peak the BOB filtered frequency shows clear evolution, allowing it to model the filtered NR waveform for longer after the peak.

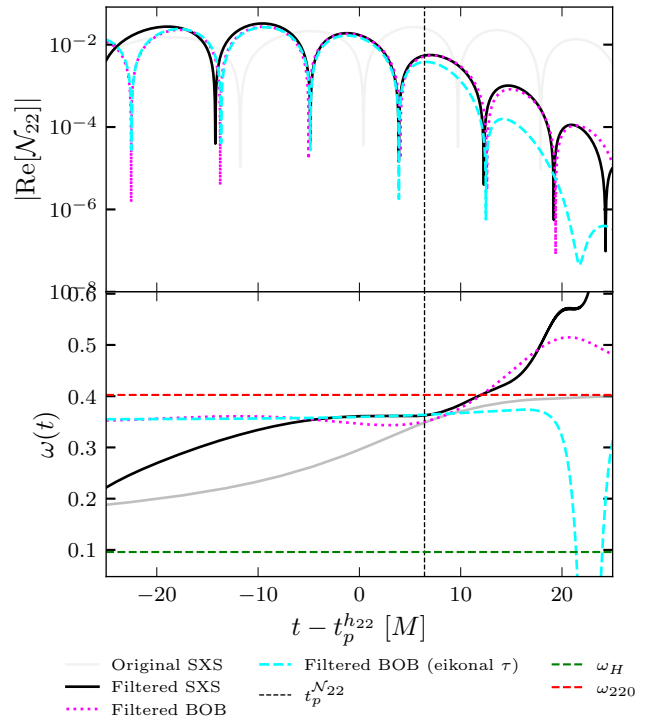


FIG. 3: Top: Filtered NR News (SXS:BBH:2477 [40–42, 45, 46]) waveform (solid black) compared to a filtered BOB waveform with the exact same QNMs removed (dotted red) and an “eikonal filtered” BOB waveform (dashed cyan). In light grey we plot the original NR waveform. Bottom: Instantaneous waveform frequency for the filtered waveforms. We also plot the qnm frequency (dashed green) and $w_H = 2\Omega_H$, where Ω_H is the horizon frequency (dashed red).

The authors of [21] interpret the direct wave as prompt emission during plunge and a model for the direct wave was developed based on the orbital dynamics of a plunging perturber. In the EMRI limit, one expects the perturber to approach the remnant horizon frequency at high spin. While the exact horizon frequency is expected to be screened, the direct wave frequency is expected to oscillate around the horizon frequency. This physical picture was used successfully to model the direct wave component of SXS:BBH:0305 in [21] and uncover the direct wave component in GW250114 [48–50] in [51]. For SXS:BBH:0305, analyzed in Fig. (1), the BOB filtered frequencies are near the horizon frequency, consistent with the physical picture in [21]. However, for the high remnant spin system, SXS:BBH:4123, both the NR and BOB filtered waveforms are well below the horizon frequency, and do not approach the horizon frequency until $20M$ after the strain peak. Because the fundamental QNM frequency ω_{220} and the horizon frequency are similar for high spins, it is further unclear if the filtered wave-

form at late times is approaching the horizon or the QNM frequency. For the high mass ratio and low remnant spin system SXS:BBH:2477, analyzed in Fig.(3), the filtered frequency is quite far from the horizon frequency. This is expected as the direct wave frequency is only expected to be around the horizon frequency for high spin systems, where frame dragging effects are strongest. Through these 3 systems, it is clear that BOB successfully models the direct wave component across initial mass ratios and remnant spins. The significant distance of both the NR and BOB filtered frequencies in both low and high remnant spin systems, suggests that the direct wave may be unrelated to the horizon frequency for comparable mass systems. To test this systematically, we compute the mean frequency of the “eikonal filtered” BOB waveform from the peak of $|\text{Re}[\mathcal{N}_{22}]|$ to $10M$ afterwards. We find our results are not sensitive to the exact boundaries of our interval, and the median, maximum and minimum frequency during this period do not show significant deviations from the average quantities, indicating we are correctly identifying the stable frequency in the “eikonal filtered” BOB waveform.

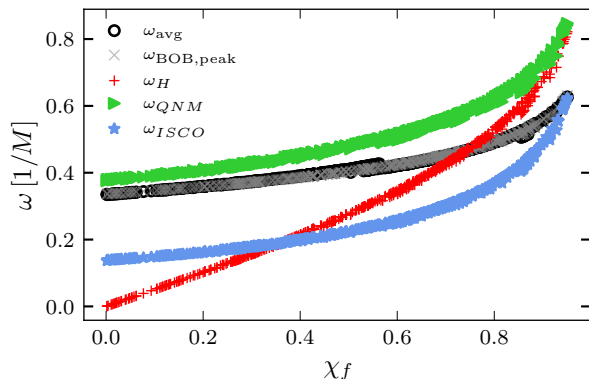


FIG. 4: Comparison of the mean “eikonal filtered” direct wave frequency (black circle) for the News with the BOB prediction for the News frequency at the time of the peak News amplitude (grey cross), $\omega_H = 2\Omega_H$, where Ω_H is the horizon frequency (red plus), real part of the $(s = -2, l = 2, m = 2, n = 0)$ qnm frequency and $\omega_{\text{ISCO}} = 2\Omega_{\text{ISCO}}$ (blue star).

Interestingly, in Fig. (4), we find that ω_{avg} follows the frequency predicted by BOB at the time of the peak News amplitude. Furthermore, there is little correlation between the BOB predicted direct wave frequency and the horizon frequency, other than an incidental crossing around $\chi_f = 0.7$. With a final spin of $\chi_f = 0.692$, SXS:BBH:0305 represents a system where the horizon frequency and the direct wave frequency happen to share similar values. This explains why direct wave frequency models based on oscillations near the horizon frequency are able to successfully model SXS:BBH:0305 [21] and

GW250114 [51], which consists of a final spin, $\chi_f = 0.68$.

Discussion.— In this work we have shown that the amplitude evolution of the Backwards One Body (BOB) model can be derived analytically from black-hole perturbation theory using the Sasaki–Nakamura formalism with the Pöschl–Teller potential. We demonstrate that the QNM pole contribution resums, to a very good approximation, to a hyperbolic secant envelope. This derivation is based on the observation that the source term $I(\omega_n, r)$ is largely independent of n , an insight supported by recent findings obtained from analyzing NR waveforms [7, 8, 34, 35]. The remarkable accuracy of BOB across the SXS catalog for quasi-circular, non-precessing systems further suggests that the source excitation is largely insensitive to the overtone index [27].

To understand why BOB can outperform QNM-based models prior to and around the waveform peak, we applied rational filters to both BOB and NR News waveforms. We analyze three SXS cases, a GW150914-like case, a $q = 4$ high remnant spin case, and a $q = 15$ low remnant spin case. In all 3 cases, we find BOB accurately models the non-QNM content of the merger radiation for an extended period of time, including before the News peak, explaining BOB’s success around the waveform peak.

In [21], based on EMRI waveforms and the GW150914-like SXS:BBH:0305, the direct wave was shown to exhibit a quasi-stable frequency close to, but not exactly at, the horizon frequency for high spin remnants. [51] used this model to extract the direct wave component from GW250114. Similar to [21], we find that the direct wave has a quasi-stable frequency, with a slow time-dependent evolution. Because of BOB’s analytical form, we are able to easily extract this quasi-stable frequency across the SXS catalog. We find that the quasi-stable frequency is uncorrelated with the horizon frequency, even for high remnant spins. Rather, there is a strong correlation with the News frequency at the time of the peak News amplitude. Around $\chi_f \approx 0.7$, the two frequencies happen to coincide, explaining why systems such as SXS:BBH:0305 and GW250114 exhibit a direct wave frequency near the horizon frequency.

Although BOB was originally motivated by perturbations of null geodesics near the light ring [6, 26], the direct wave has been associated with radiation emitted by a plunging timelike perturber. The ability of BOB to accurately model this prompt emission suggests that outgoing rays from the plunging source are well modeled by a null-geodesic description. Our results suggest that BOB effectively captures the QNM and direct wave contributions to the merger-ringdown radiation, while requiring only 4 parameters, M_f, χ_f, A_p and Ω_0 . While our analytical results are based on the simpler Pöschl–Teller potential, the success of BOB for quasi-circular and non-precessing systems across the SXS catalog [27] suggests that the physical intuition obtained from this simpler model extends

to the Kerr case. These results, in combination with recent analytical advances in isolating the non-QNM pole contribution [36, 52], suggest that connecting BOB analytically to both the direct and QNM pole contributions is a promising direction for future work.

Acknowledgements.— AK thanks Sizheng Ma for helpful discussions and pointing out work on direct waves and rational filters. AK and STM were supported in part by NASA grants 22-LPS22-0022 and 24-2024EPSCoR-0010. The authors acknowledge the computational resources provided by the WVU Research Computing Thorny Flat HPC cluster, which is funded in part by NSF OAC-1726534.

SUPPLEMENTAL MATERIAL

SN formalism

Here we provide an overview of the SN formalism, following [33]. We take $G = c = 2M = 1$. Starting with Eq. (1) and assuming the observer is located far from the black hole, we can approximate $\hat{X}^{(s)}(\omega, r)$ as

$$\hat{X}^{(s)}(\omega, r) \approx \frac{e^{i\omega r_*}}{2i\omega A_{\text{in}}(\omega)} \int_{-\infty}^{+\infty} I(\omega, r'_*) \hat{X}_{r'_+}^{(s)}(\omega, r'_*) dr'_* \quad (11)$$

where $\hat{X}_{r'_+}^{(s)}$ is subject to the boundary conditions

$$\lim_{r \rightarrow r_+} \hat{X}_{r_+}^{(s)} \sim e^{-i(\omega - m\Omega)r_*} \quad (12)$$

$$\lim_{r \rightarrow \infty} \hat{X}_{r_+}^{(s)} \sim A_{\text{in}}(\omega) e^{-i\omega r_*} + A_{\text{out}}(\omega) e^{i\omega r_*} \quad (13)$$

The subsequent contour integration has to be taken with care to make sure only the QNM contributions are included. The QNM contribution can then be written as

$$X^{(s)}(t, r) = -\text{Re} \left[\sum_n B_n e^{-i\omega_n(t-r_*)} \int_{-\infty}^{\infty} \frac{I(\omega, r'_*) \hat{X}_{r'_+}^{(s)}}{A_{\text{out}}} dr'_* \right] \quad (14)$$

where B_n are the quasinormal excitation factors, defined as

$$B_n = \frac{A_{\text{out}}(\omega)}{2\omega} \left(\frac{dA_{\text{in}}}{d\omega} \right)^{-1} \Big|_{\omega=\omega_n} \quad (15)$$

Defining the quasinormal excitation coefficients C_n as

$$C_n = B_n \int_{-\infty}^{+\infty} \frac{I(\omega, r'_*) \hat{X}_{r'_+}^{(s)}}{A_{\text{out}}} dr'_* \quad (16)$$

we obtain the standard description of the ringdown as a sum of quasinormal modes.

$$X^{(s)}(t, r) = -\text{Re} \left[\sum_n C_n e^{-i\omega_n(t-r_*)} \right] \quad (17)$$

To relate the master variable X to the gravitational wave strain h as $r \rightarrow \infty$, we follow [33, 38] for a non-spinning black hole, $a = 0, s = -2$.

$$h_+(t) - ih_\times(t) = \frac{8}{r} \sum_{lm} -{}_2Y_{lm}(\theta, \phi) \int_{-\infty}^{\infty} \frac{\hat{X}^{(-2)}}{c_0(\omega)} e^{-i\omega t} d\omega, \quad (18)$$

where $c_0 = -12i\omega + l(l+1)(l(l+1)-2)$ for $a = 0, s = -2$. To go from Eq. (7) to Eq. (9) we assume the eikonal limit where $c_0 \propto l^2$, although we can see even for $l = 2$ the real part is significantly larger. This allows us to move c_0 to outside the integral and solve the integral for the PT potential using the same derivation as in the main text. However, for non-spinning systems, we can approximate the leading order correction due to the imaginary part of c_0 by treating it in the time domain. Noting that

$$\int_{-\infty}^{\infty} \frac{\hat{f}(\omega)}{c_0(\omega)} e^{-i\omega t} d\omega = \frac{1}{c_0(i\partial_t)} f(t) \quad (19)$$

and

$$c_0(i\partial_t)[e^{i\alpha\delta t} f(t)] = e^{i\alpha\delta t} c_0(i\partial_t - \alpha\delta) f(t), \quad (20)$$

we can use $1/(A + Bx) \approx 1/A(1 - Bx/A)$ and Taylor expand $c_0(i\partial_t - \alpha\delta)$ to obtain a leading order correction to the BOB evolution

$$\mathcal{N}(t) = A_p \text{sech} \left(\frac{t - t_p}{\tau} \right) \left[1 + \frac{2 - i \text{Re}(\omega_{220})}{\tau(4 + \text{Re}(\omega_{220})^2)} \tanh \left(\frac{t - t_p}{\tau} \right) \right] e^{i\Phi}, \quad (21)$$

where Φ is the original BOB phase evolution and we have replaced the PT QNMs with the full Kerr QNMs. Testing across the SXS catalog for quasi-circular and non-precessing systems, we find mixed performance. This is unsurprising considering Eq. (21) is an approximation of the full non-spinning correction, and we are testing against spinning remnants. In [27], it was found that BOB showed the worst mismatches for systems with $\chi_{\text{eff}} \gtrsim 0$ and $q \gg 1$. Interestingly, we find this correction consistently improves BOB's accuracy in this area of the parameter space. Evaluated against 53 cases in the SXS catalog with $q \geq 5$ and $\chi_{\text{eff}} \geq 0$, we find the mean mismatch decreases from 1.94×10^{-4} to 7.59×10^{-5} and the median mismatch decreases from 1.6×10^{-4} to 4.28×10^{-5} . These results suggest incorporating the full spin effects in the transformation from X to \mathcal{N} may result in corrections to BOB that significantly improve its accuracy across the parameter space.

Hypergeometric Function

While BOB predicts a hyperbolic secant amplitude profile, our final result in Eq. (7) involves the product

of a hyperbolic secant and a hypergeometric function

$$F(-\beta, -1 - \beta, -2\beta; e^{-\alpha(t-r_*)}) = \sum_{n=0}^{\infty} \frac{(-\beta)_n (-1 - \beta)_n e^{-n\alpha(t-r_*)}}{(-2\beta)_n n!}, \quad (22)$$

where $(x)_n = \Gamma(x+n)/\Gamma(x)$ is the Pochhammer symbol. Because our hypergeometric function very quickly asymptotes to a constant, due to $z = e^{-\alpha(t-r_*)}$, we treat $|F|$ as a constant in our derivation, allowing us to reproduce the BOB hyperbolic secant profile exactly.

The PT potential can be tuned to mimic the Zerilli potential near the peak with parameter choices $x_0 = 0.95$, $V_0 = 0.605$ and $\alpha = 0.362$ [36]. In Fig. 5 we show the pure hyperbolic secant profile predicted by BOB, $\text{sech}(t/\tau)$, and the hypergeometric corrected profile $|F(-\beta, -1 - \beta, -2\beta; e^{-\alpha(t-r_*)})|\text{sech}(t/\tau)$. Both profiles are normalized to a maximum value of 1, due to the freedom allowed by the overall normalization parameter A_p present in BOB, and the hypergeometric profile is timeshifted by x_0 , corresponding to the shift in the peak of the PT potential. As can be seen in Fig. 5, the two profiles show excellent agreement, with a very small disagreement near the peak. While this shows that treating $|F|$ as a constant does not significantly impact our amplitude profile, this derivation suggests that a hypergeometric correction is physically motivated and will likely lead to more accurate corrections to BOB in the future.

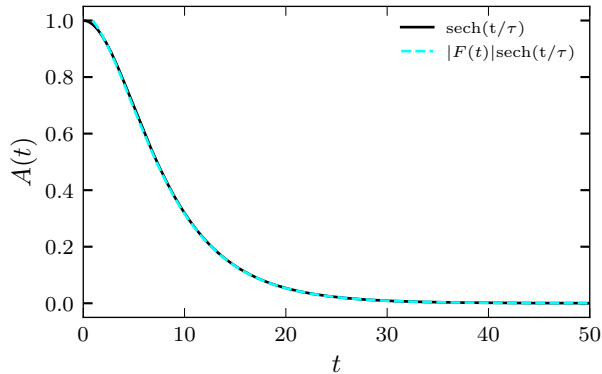


FIG. 5: Comparison of $\text{sech}(t/\tau)$ (solid black) and $|F(t)|\text{sech}(t/\tau)$ where $F(t)$ is the hypergeometric function appearing in Eq. (7).

* anuj.kankani@mail.wvu.edu

- [1] T. Regge and J. A. Wheeler, *Physical Review* **108**, 1063 (1957).
 [2] C. Vishveshwara, *Nature* **227**, 936 (1970).
 [3] S. A. Teukolsky, *Physical Review Letters* **29**, 1114 (1972).
 [4] K. D. Kokkotas and B. G. Schmidt, *Living Reviews in Relativity* **2**, 2 (1999).

- [5] E. Berti, V. Cardoso, and A. O. Starinets, *Classical and Quantum Gravity* **26**, 163001 (2009).
 [6] V. Ferrari and B. Mashhoon, *Physical Review D* **30**, 295 (1984).
 [7] M. Giesler, M. Isi, M. A. Scheel, and S. A. Teukolsky, *Physical Review X* **9**, 041060 (2019).
 [8] M. H.-Y. Cheung, E. Berti, V. Baibhav, and R. Cotesta, *Physical Review D* **109**, 044069 (2024).
 [9] C. Pacilio, S. Bhagwat, F. Nobili, and D. Gerosa, *Physical Review D* **110**, 103037 (2024).
 [10] V. Baibhav, M. H.-Y. Cheung, E. Berti, V. Cardoso, G. Carullo, R. Cotesta, W. Del Pozzo, and F. Duque, *Physical Review D* **108**, 104020 (2023).
 [11] L. Magaña Zertuche, L. C. Stein, K. Mitman, S. E. Field, V. Varma, M. Boyle, N. Deppe, L. E. Kidder, J. Moxon, H. P. Pfeiffer, *et al.*, *Physical Review D* **112**, 024077 (2025).
 [12] K. Mitman, M. Lagos, L. C. Stein, S. Ma, L. Hui, Y. Chen, N. Deppe, F. Hébert, L. E. Kidder, J. Moxon, *et al.*, *Physical Review Letters* **130**, 081402 (2023).
 [13] M. H.-Y. Cheung, V. Baibhav, E. Berti, V. Cardoso, G. Carullo, R. Cotesta, W. Del Pozzo, F. Duque, T. Helfer, E. Shukla, *et al.*, *Physical Review Letters* **130**, 081401 (2023).
 [14] S. Ma and H. Yang, *Physical Review D* **109**, 104070 (2024).
 [15] H. Zhu, J. L. Ripley, F. Pretorius, S. Ma, K. Mitman, R. Owen, M. Boyle, Y. Chen, N. Deppe, L. E. Kidder, *et al.*, *Physical Review D* **109**, 104050 (2024).
 [16] J. Redondo-Yuste, G. Carullo, J. L. Ripley, E. Berti, and V. Cardoso, *Physical Review D* **109**, L101503 (2024).
 [17] B. Bucciotti, L. Juliano, A. Kuntz, and E. Trincerini, *Physical Review D* **110**, 104048 (2024).
 [18] S. Ma, M. A. Scheel, J. Moxon, K. C. Nelli, N. Deppe, L. E. Kidder, W. Throwe, and N. L. Vu, *Physical Review D* **112**, 024003 (2025).
 [19] M. De Amicis, H. R. Rüter, G. Carullo, S. Albanesi, C. Melize Ferrus, K. Mitman, L. C. Stein, V. Cardoso, S. Bernuzzi, M. Boyle, *et al.*, *Physical Review Letters* **135**, 171401 (2025).
 [20] T. Islam, G. Faggioli, G. Khanna, S. E. Field, M. van de Meent, and A. Buonanno, *Physical Review D* **112**, 024061 (2025).
 [21] N. Oshita, S. Ma, Y. Chen, and H. Yang, arXiv preprint arXiv:2509.09165 (2025).
 [22] S. Ma, K. Mitman, L. Sun, N. Deppe, F. Hébert, L. E. Kidder, J. Moxon, W. Throwe, N. L. Vu, and Y. Chen, *Physical Review D* **106**, 084036 (2022).
 [23] S. Ma, L. Sun, and Y. Chen, *Physical Review Letters* **130**, 141401 (2023).
 [24] S. Ma, L. Sun, and Y. Chen, *Physical Review D* **107**, 084010 (2023).
 [25] N. Lu, S. Ma, O. J. Piccinni, L. Sun, and E. Finch, *Physical Review D* **112**, 064047 (2025).
 [26] S. T. McWilliams, *Physical review letters* **122**, 191102 (2019).
 [27] A. Kankani and S. T. McWilliams, arXiv preprint arXiv:2510.25012 (2025).
 [28] A. Kankani and S. T. McWilliams, *Phys. Rev. D* **112**, 124051 (2025).
 [29] S. Mahesh, S. T. McWilliams, and Z. Etienne, *Physical Review D* **112**, 124065 (2025).
 [30] S. Ma, M. Giesler, V. Varma, M. A. Scheel, and Y. Chen, *Physical Review D* **104**, 084003 (2021).

- [31] G. Pöschl and E. Teller, *Zeitschrift für Physik* **83**, 143 (1933).
- [32] M. Sasaki and T. Nakamura, *Progress of Theoretical Physics* **67**, 1788 (1982).
- [33] E. Berti and V. Cardoso, *Physical Review D—Particles, Fields, Gravitation, and Cosmology* **74**, 104020 (2006).
- [34] K. Mitman, I. Pretto, H. Siegel, M. A. Scheel, S. A. Teukolsky, M. Boyle, N. Deppe, L. E. Kidder, J. Moxon, K. C. Nelli, *et al.*, *Physical Review D* **112**, 064016 (2025).
- [35] N. Oshita, *Physical Review D* **104**, 124032 (2021).
- [36] A. Kuntz, arXiv preprint arXiv:2510.17954 (2025).
- [37] DLMF §15.2, §15.2: *Definitions and Analytical Properties*, nist digital library of mathematical functions, <https://dlmf.nist.gov/15.2>, Release 1.2.5 of 2025 12 15 (2025).
- [38] Y. Yin, R. K. Lo, and X. Chen, arXiv preprint arXiv:2511.08673 (2025).
- [39] SXS Collaboration, Binary black-hole simulation SXS:BBH:0305 (2025).
- [40] SXS Collaboration, The sxs catalog of simulations v3.0.0 (2025).
- [41] M. Boyle, K. Mitman, M. Scheel, and L. Stein, The sxs package (2025).
- [42] M. A. Scheel, M. Boyle, K. Mitman, N. Deppe, L. C. Stein, C. Armaza, M. S. Bonilla, L. T. Buchman, A. Ceja, H. Chaudhary, *et al.*, *Classical and Quantum Gravity* **42**, 195017 (2025).
- [43] B. P. Abbott, R. Abbott, T. D. Abbott, M. R. Abernathy, F. Acernese, K. Ackley, C. Adams, T. Adams, P. Addesso, R. X. Adhikari, *et al.*, *Physical review letters* **116**, 061102 (2016).
- [44] SXS Collaboration, Binary black-hole simulation SXS:BBH:4123 (2025).
- [45] J. Yoo, V. Varma, M. Giesler, M. A. Scheel, C.-J. Haster, H. P. Pfeiffer, L. E. Kidder, and M. Boyle, *Physical Review D* **106**, 10.1103/physrevd.106.044001 (2022).
- [46] SXS Collaboration, Binary black-hole simulation SXS:BBH:2477 (2025).
- [47] L. C. Stein, arXiv preprint arXiv:1908.10377 (2019).
- [48] A. Abac, I. Abouelfettouh, F. Acernese, K. Ackley, C. Adamcewicz, S. Adhicary, D. Adhikari, N. Adhikari, R. Adhikari, V. Adkins, *et al.*, arXiv preprint arXiv:2508.18079 (2025).
- [49] A. Abac, I. Abouelfettouh, F. Acernese, K. Ackley, C. Adamcewicz, S. Adhicary, D. Adhikari, N. Adhikari, R. Adhikari, V. Adkins, *et al.*, *Physical review letters* **136**, 041403 (2026).
- [50] A. Abac, I. Abouelfettouh, F. Acernese, K. Ackley, C. Adamcewicz, S. Adhicary, D. Adhikari, N. Adhikari, R. Adhikari, V. Adkins, *et al.*, *Physical review letters* **135**, 111403 (2025).
- [51] N. Lu, S. Ma, O. J. Piccinni, Y. Chen, and L. Sun, arXiv preprint arXiv:2510.01001 (2025).
- [52] J. Su, N. Khera, M. Casals, S. Ma, A. Chowdhuri, and H. Yang, arXiv preprint arXiv:2601.22015 (2026).